Microscale diffusiophoresis of proteins

Quentin Peter
University of Cambridge https://orcid.org/0000-0002-8018-3059
Raphaël Jacquat
University of Cambridge
Therese Herling
University of Cambridge
Pavan Challa
University of Cambridge
Tadas Kartanas
University of Cambridge
Tuomas Knowles (tpjk2@cam.ac.uk)
University of Cambridge https://orcid.org/0000-0002-7879-0140

Article

Keywords: microfluidic measurements, proteins, diffusiophoretic motion, salt gradients, microfluidics devices, spatial organisation of macromolecules

Posted Date: October 20th, 2020

DOI: https://doi.org/10.21203/rs.3.rs-90645/v1

Microscale diffusiophoresis of proteins

Quentin Peter[1,†], Raphael Jacquat[2,†], Therese W. Herling[1], Pavan Kumar Challa[1], Tadas Kartanas[1] & Tuomas P. J. Knowles[1,2]

[†] *These authors contributed equally to this work.*

[1] *Department of Chemistry, University of Cambridge, Lensfield Road, CB2 1EW, Cambridge, UK.*

[2] *Cavendish Laboratory, Department of Physics, University of Cambridge, JJ Thomson Avenue, CB3 0HE, Cambridge, UK.*

Living systems are characterised by their spatially highly inhomogeneous nature which is susceptible to modify fundamentally the behaviour of biomolecular species, including the proteins that underpin biological functionality in cells. Spatial gradients in chemical potential are known to lead to strong transport effects for colloidal particles, but their effect on molecular scale species such as proteins has remained largely unexplored. Here we demonstrate with microfluidic measurements that individual proteins can undergo strong diffusiophoretic motion in salt gradients in a manner which is sufficient to overcome diffusion and lead to dramatic changes in their spatial organisation on the scale of a cell. Moreover, we demonstrate that this phenomenon can be used to control the motion of proteins in microfluidics devices. These results open up a path towards a physical understanding of the role of gradients in living systems in the spatial organisation of macromolecules and highlight novel routes towards protein sorting applications on device.

Living cells constantly work to remain out of equilibrium, a key requirement for life. One

crucial aspect of the non-equilibrium nature of living systems is the ubiquitous presence of gradients in ionic strength, maintained using ion pumps and related molecular machinery. This situation is fundamentally different to the spatially largely homogeneous conditions that characterise protein studies *in vitro* under bulk solution conditions. Understanding the diffusiophoresis of proteins can therefore yield insights in the nature and regulation of protein transport in living organisms. Although over the past few decades diffusiophoresis has been well studied for larger colloids [1–4], very little is known about whether single protein molecules, which are much smaller than typical colloids, can also undergo diffusiophoresis and which factors can modulate this process. In biophysics and life sciences, microfluidic techniques are increasingly used to probe the nature of proteins [5–9]. The rapid growth of the use of microfluidic techniques in research and industry[10,11] is in part motivated by the fact that, compared to bulk processes, microfluidic processes enable a significant decrease in the required volume of solution. Moreover, under the microfluidic regime it is possible to create laminar flows[12], which enable a fine control of dynamic experiments and allow measurements which are often not possible in bulk solution. Similar phoretic processes, electrophoresis[13,14] and thermophoresis[15,16] are used to develop novel microfluidic techniques in research and industry.

In this study, we explore protein diffusiophoresis using a microfluidic format which allows to control protein mass transport by eliminating the influence of factors such as convection which are ubiquitous in bulk measurements. Previous geometries used for the study of diffusiophoresis of colloids include two channels merging perpendicularly [17] or two parallel channels joined by a micro-[18] or nano-channel[19]. Here we exploit a simple geometry consisting of a dead-end perpen-

dicular to a main channel[20]. Measuring the key properties of proteins such as mobility, size, and isoelectric point of proteins is one of the main goals in developing tools for protein science. Diffusiophoresis can used for sizing [20] colloids and calculating their ζ-potential [21] in microfluidics, and could therefore be extremely useful if this effect is significant for proteins.

Results and Discussion

In order to explore whether or not proteins undergo a significant level of diffusiophoresis, we designed a microfluidic device that enables the generation of a localised solute gradient. The experiment is illustrated in Figure (1). After filling the device with a high solute concentration, this geometry allows the content of the main channel to be replaced by a protein solution with low ion concentration, while maintaining the high salt concentration in the dead-end. A strong solute gradient is therefore created at the dead-end inlet. The propagation of proteins over time in this solute gradient is captured by a UV-based autofluorescence microscope enabling label-free measurement of protein concentration[22]. The data in Figure (1C) reveals a very significant effect on protein mass transport resulting from this solute gradient.

In order to understand the origin of this remarkably large diffusiophoretic effect, we consider the key physical parameters governing the motion of large scale objects such as colloids which exhibit two principal contributions to diffusiophoresis: electrophoresis and chemiophoresis (see the methods section). To investigate whether such effects or other related phenomena play a role for the behaviour of protein which are a factor $10^5 - 10^6$ smaller in volume than typical colloids,

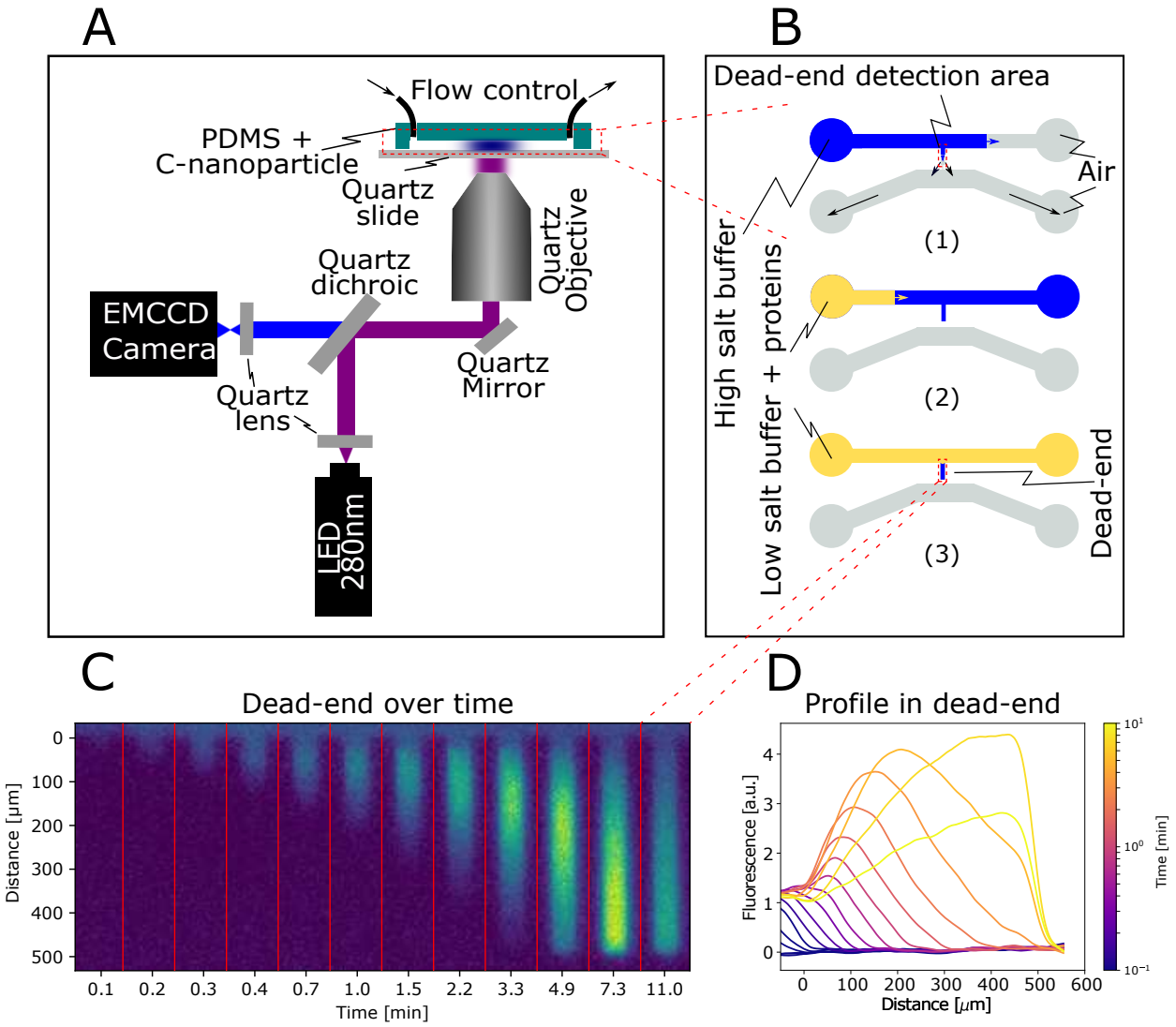

Figure 1: (A) Schematic of the UV label-free microscope used to image a microfluidic device with a dead-end geometry. (B) Microfluidic device design used in this study. (B1) Firstly, the device is filled with a high-salt buffer. The air in the dead-end is pushed through the PDMS in an empty lower channel. (B2) A protein solution is then pushed in the main channel, (B3) leaving the high salt solution only inside the dead-end. (C) A video of the dead-end is taken with logarithmically spaced time points to reduce photobleaching. (D) The channel is detected in each frame and the average over the width is extracted to form a profile.

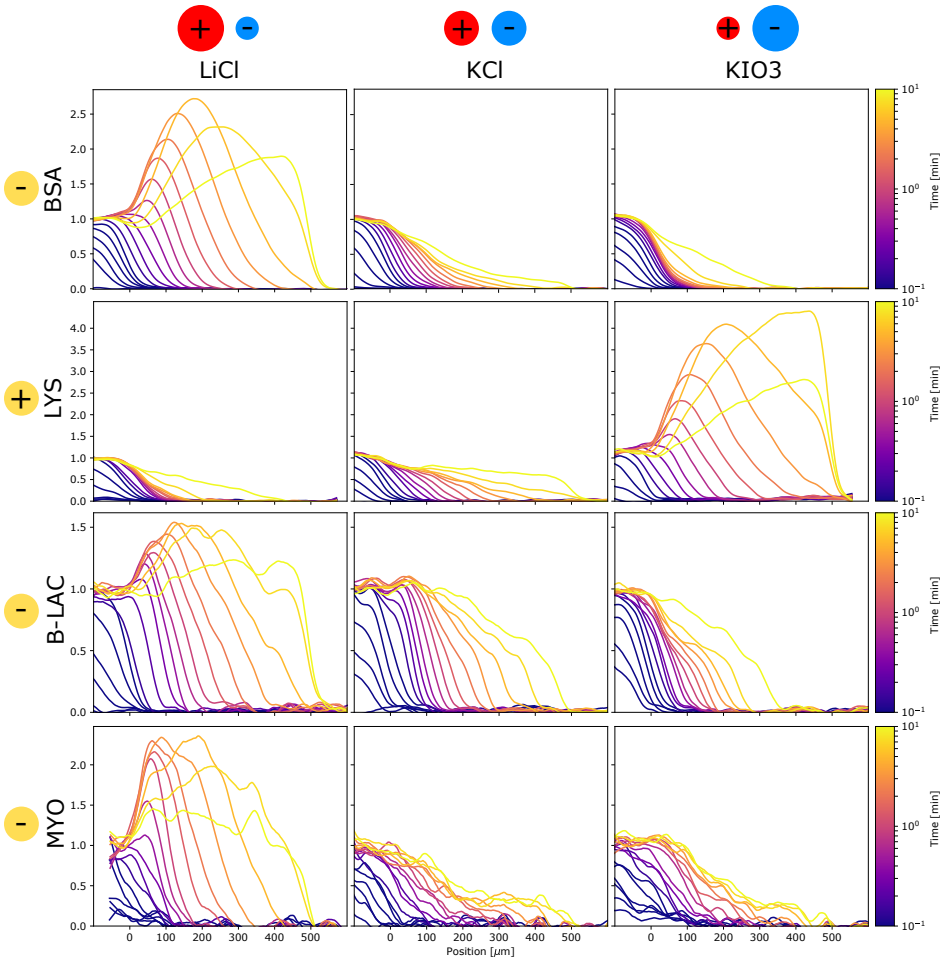

Figure 2: Diffusiophoresis of proteins in different salt gradients. Three negatively charged protein, Bovine Serum Albumin (BSA), Beta-Lactoglobulin (B − LAC), and Myoglobin (MYO), as well as a positively charged protein, Lysozyme (LYS), are placed into a salt gradient. The salts used to create this gradient are Lithium chloride (LiCl), Potassium chloride (KCl), and Potassium iodate (KIO_3). If the more diffusive salt ion has the same charge as the protein, a concentration peak appears in the channel. When the more diffusive salt ion has the same charge as the protein, the diffusion in the channel is reduced. If the two ions have similar diffusivity, no effect is visible. A sketch of the ions is shown on top of the figure to help visualize the relative diffusivities, where smaller means more diffusive.

we selected a range of proteins and salts. In particular, we selected the conjugated salts from strong bases and acids to avoid affecting the pH of the solution. We first focus on LiCl and $\mathrm{KIO_3}$, which have a strong difference in the diffusion coefficient of the ions, and on KCl, whose ions have similar diffusivities. This differential behaviour is captured by the β coefficient which is the normalised difference between the ionic diffusion coefficients D_+ and D_-: $\beta \equiv (D_+ - D_-)(D_+ + D_-)^{-1}$. For example, LiCl has $D_{Li^+} = 1.03 \cdot 10^{-8} m^2/s$ and $D_{Cl^-} = 2.03 \cdot 10^{-8} m^2/s$, which gives a normalised difference of $\beta = -0.326$. The β coefficient of $\mathrm{KIO_3}$ (0.298) is roughly equal and opposite, and KCl (-0.019) is much smaller[23]. Our experiments were designed to test whether the electrophoresis term dominates, resulting in a strong and opposite effect from LiCl and $\mathrm{KIO_3}$, or if the chemiophoresis term dominates, resulting in a similar effect from all three salts. The results are shown in Figure (2). The first column shows LiCl which dissolves into a more diffusive $\mathrm{Cl^-}$ anion and a less diffusive $\mathrm{Li^+}$ cation. An electric field pointing out of the dead end is created by the difference in the ionic diffusion to avoid charge separation. Consistently with the electrophoretic description, bovine serum albumin (BSA), whose charge is negative at pH 7, is attracted and concentrated in the dead-end, forming a visible concentrated peak. The data in the first column of Figure (2) further reveal that Lysozyme (LYS), whose charge is positive at pH 7, is by contrast prevented from entering the channel for a few minutes, until the strength of the salt gradient decreases. We next investigated the effect of KCl whose ions have approximatively the same size in the second column of Figure (2). The profiles are consistent with diffusion alone and the diffusiophoretic effect is not significant. To verify this conclusion, a third salt was tested. $\mathrm{KIO_3}$ creates a roughly equal and opposite electric field compared with LiCl. As expected, the third

column of Figure (2) reveals that BSA diffusion into the dead-end is significantly restricted for several minutes. Lysozyme is instead strongly concentrated and attracted into the dead-end. This result highlight the role of electrostatics and indicates that the electrophoresis is much stronger than the chemiophoretic contribution. More proteins have been tested and are shown in the SI.

In the attractive case, a concentration peak becomes visible. The position of the peak depends mostly on the diffusiophoresis strength and the width of the peak depends on the protein size. This opens up the possibility to fit the peaks to extract these informations about the proteins. We can capture the physics in one dimensional space by introducing a dimensionless parameter[24], $\eta = x/\sqrt{4D_s t}$ describing distances x relative to the mean diffusional distance of the salt with diffusion coefficient D_s at a time t. The protein concentration (N) depends on the diffusion ($D_p d^2N/d\eta^2$) and on a driving force from the gradient in the channel potential of the salt creating a dimensionless velocity ($d\ln C/d\eta$):

$$\frac{D_p}{D_s}\frac{d^2N}{d\eta^2} + 2\eta\frac{dN}{d\eta} - \frac{\Gamma_p}{D_s}\frac{d}{d\eta}\left(N\frac{d\ln C}{d\eta}\right) = 0 \tag{1}$$

The dimensionless constants represent the ratio of the protein diffusion coefficient (D_p) and diffusiophoretic coefficient (Γ_p) with the salt diffusion coefficient (D_s). The salt diffusion coefficient captures the diffusion of both ions which results to a weighted average of the ionic diffusivities. The diffusiophoretic coefficient depends on the protein and on the salt properties. In the dilute limit, the salt concentration C is given by a single constant (α), which is the ratio of the concentration in the main channel by the initial concentration in the dead-end:

$$C(\eta) = \alpha + (1-\alpha)\,\mathrm{erf}(\eta) \tag{2}$$

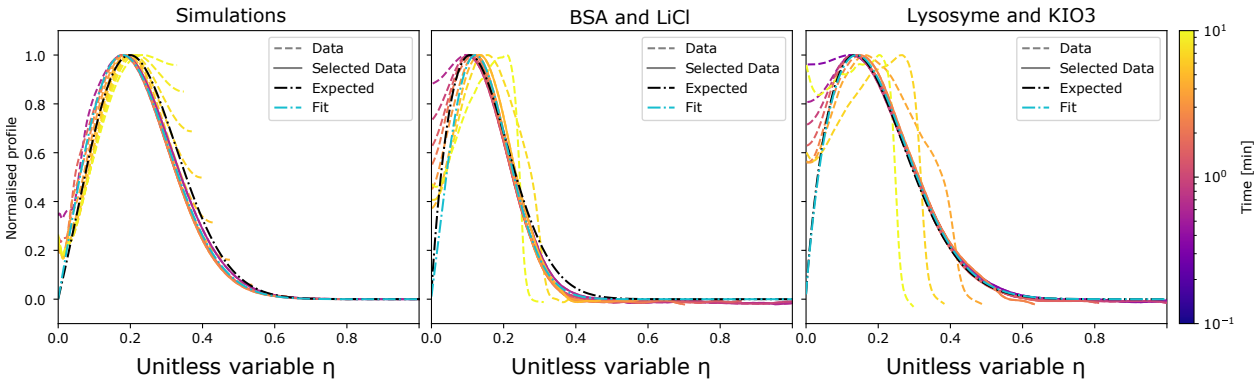

Figure 3: Quantitative description of diffusiophoresis. A finite elements simulation and the two proteins from Figure (2) are plotted as a function of the dimensionless variable η. The finite elements simulation and the measurements give similar results. Most curves overlap with the 1D model. The differences are explained by two effects. The main channel is not a perfect reservoir, which can be seen on the left near $\eta = 0$. The dead-end channel is not semi-infinite, which is seen by the later, yellow curves not overlapping when reaching the end of the channel. The fitted profile (cyan) and the expected profile (black) both are a good match to the profiles.

Interestingly, this simple one-dimensional analysis predicts qualitatively the observed trends, thus capturing the essential physics, as shown in Figure (3). A quantitative comparison reveals that the predicted peak heights are higher than those observed in the experiments. To understand the origin of this effect, we next performed finite elements simulations for multidimensional systems. The reason for the observed differences in the peak heights is a depletion of analyte at the inlet of the dead-end that is not captured in the one dimensional analysis. However, when normalized by the height of the concentration peak, the profiles have the same shape, as illustrated in Figure (3). The cyan profiles, fitted with Equation (1), match well the measurements and finite elements simulations. The width of the peak is directly related to the proteins diffusion coefficient, and the protein mobility can be obtained from the location of the peak. The black profiles in Figure (3) indicates the expected curves from the mobility and radius measured by free flow electrophoresis [25] and diffusional sizing [26].

The finite elements simulations have been validated by experiments and give us an opportunity to query which experimental parameters can be optimized for future developments to maximise the strength of the diffusiophoretic effect. For example, these simulations show how the concentration power depends on the salt properties. Figure (4) summarises the strength of the effect while varying different experimental parameters. First, we investigate the effect of the salt concentration ratio between the main channel and the initial dead-end concentration (4A). A ratio of one leads as expected to no diffusiophoretic effect. As the ratio decreases, the effect becomes stronger but rapidly saturates when the main channel molarity is two to three order of magnitude below the dead-end molarity. Next, a protein with large diffusion coefficient is unsurprisingly

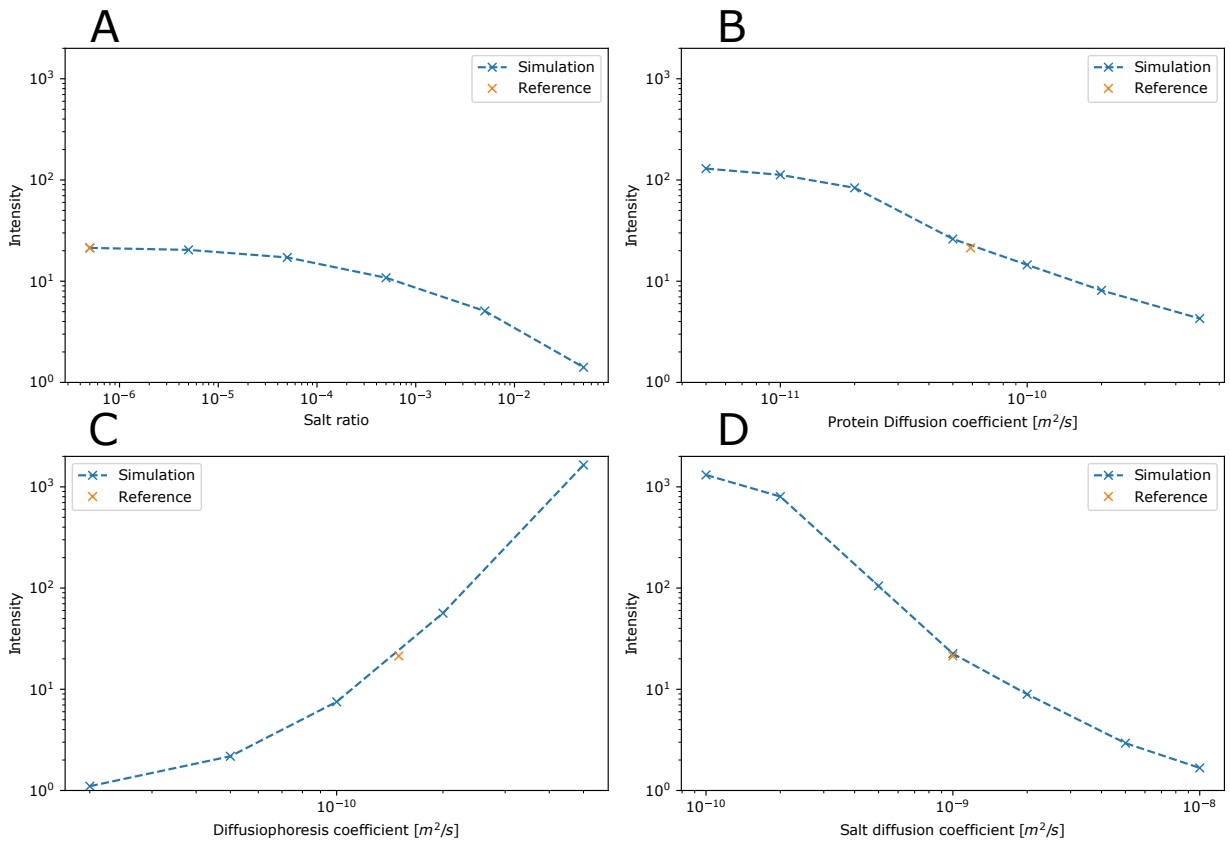

Figure 4: Role of the physical properties of proteins on the strength of the diffusiophoresis effect. The maximum concentration of the simulations is shown as a function of (A) salt ratio, (B) protein diffusion coefficient, (C) diffusiophoresis coefficient, and (D) salt diffusion coefficient. The intensity is the ratio of the maximal concentration with the initial protein concentration. The reference value is the same between the four graphs.

harder to concentrate (Figure 4B). As expected, the diffusiophoresis coefficient is a major contributor to the concentration (Figure 4C). Therefore, to see a large effect, β should be maximised. A perhaps less intuitive result is shown in the final plot (Figure 4D). As the salt diffusion coefficient increases, the intensity decreases. This is explained in the main text in Equation (1), as the unit-less parameter that controls the diffusiophoresis is Γ_p/D_s. An experiment designed to analyse proteins using the diffusiophoretic effect should therefore use a high concentration of a salt that has both a large difference in ionic diffusion coefficient, and whose own diffusion coefficient is small. As explained in the supplementary informations, this is achieved by maximising the difference of ionic hydrodynamic radii.

Conclusion

This paper describes a direct, real-space observation of diffusiophoresis of proteins. This spatial effect is commonly ignored in descriptions of biological systems and a method to measure it could open the way to novel physiological discoveries. Diffusiophoresis, which is dependent on particle size, is significant for proteins and could have applications for the manipulation of proteins in microfluidic devices. In our diffusiophoretic experiments, we could concentrate proteins by up to a factor of four, as well as prevent them from entering the channel during several minutes. Furthermore, we are able to estimate the protein diffusion and diffusiophoretic coefficients. We could show that the electrophoretic contribution to diffusiophoresis is much more consequential than the chemiophoretic contribution. Finally, we discussed how to increase the effect by choosing a salt that is composed of ions with a large difference in relative diffusion coefficient. This opens up

the door to fundamentally new microfluidic approaches for protein detection and characterisation.

Methods

Colloids diffusiophoresis In colloids experiments, diffusiophoresis is described as a result of two effects[1]: chemiophoresis and electrophoresis. The electrophoretic motion is caused by difference of ion diffusion coefficient ($D_{\pm}$) of a salt. An electric field (E) appears between cations and anions to prevent a bulk separation. It depends on the differential ratio of the ions diffusion coefficient (β)[1]:

$$E = -\beta \frac{k_B T}{Ze} \frac{d \ln C}{dx} \qquad \beta = \frac{D_+ - D_-}{D_+ + D_-}. \tag{3}$$

Where $k_B T$ is the thermal energy and Ze is the ionic charge. The second term, the chemiophoretic contribution, is due to pressure difference inside the double layers of protein [20], which is similar to osmosis. One could note that the size of a protein it typically much smaller than the Debye length, so the applicability of this effect that has been described for large colloids might be doubtful. These two effects are described by the diffusiophoretic mobility of the protein (Γ_p) that controls the diffusiophoretic speed $u_p = \Gamma_p \nabla \ln C$. For a purely electrophoretical experiment, the diffusiophoretic mobility is proportional to the ζ-potential of the proteins (ζ_p) [20,27–29] and on the electrophoretic mobility (μ_p):

$$\Gamma_p = \zeta_p \frac{\epsilon}{\eta} \frac{k_B T}{Ze} \beta = \mu_p \frac{k_B T}{Ze} \beta \tag{4}$$

Where ϵ is the permittivity and η is the viscosity of the solvent. The diffusiophoresis therefore depends on the protein through its mobility, and on the salt through the charge of and β coefficient.

Experimental setup A microfluidic PDMS device with a dead-end geometry, shown in Figure (1), was used to create a gradient of salt. It is composed of three regions. The main channel is where the solution will be flowed and is a straight channel with cross section 500×50 μm^2. The dead-end channel is perpendicular to this channel and its dimensions are $50 \times 50 \times 500$ μm^3. A second, unconnected channel is placed near the end of the dead-end to provide an escape to the air going through the PDMS. The PDMS is casted on a master created by photo-lithography[30] and cured. It was then bounded to a quartz slide using a plasma oven.

The device is first filled with the solution which is intended for the dead-end channel. Pressure is applied until the air is evacuated through the PDMS in the second channel. A second solution is then pushed in the main channel, which comes into contact with the first solution at the base of the dead-end channel. The pressure is applied by hand for the priming of the chip and using a neMESYS syringe pump when pushing the protein solution at a flow rate of 600ulph.

A UV-LED based microscope is used to detect the proteins autofluorescence at 280nm[22]. This is important as a covalently attached label might change the key properties of the protein. In practice, the observed fluorescence intensity at longer times is systematically lower, due to photobleaching. To reduce this effect, the images are logarithmically spaced in time.

The proteins have been obtained from Sigma-Aldrich. The proteins and product numbers are Myoglobin from equine skeletal muscle (M0630), Thyroglobulin from bovine thyroid (T1001), Lysozyme from chicken egg white (L6876), β-Lactoglobulin from bovine milk (L3908), and Bovine Serum Albumin (A7906). The concentrations used where 10uM for BSA, β-Lactoglobulin, and

Lyosyme, 1uM for Thyroglobulin, and 30uM for Myoglobulin. The experiments where made with three different salt LiCl, KCl, KIO3 at 200mM. All results can be found online [1].

Channel geometry One might expect that inverting the solute concentration would result in an inversion of the diffusiophoretic velocity. In reality, the diffusiophoretic velocity u depends on $\nabla \ln(C) = \nabla C/C$ where C is the solute concentration[1]. Having the salt in the dead ends causes both the highest gradient and the lowest concentration to be localised at the inlet of the dead-end, therefore leading to the largest effect. In contrast, if the high solute concentration is in the main channel, there are only small guiding fields near the entrance, which greatly reduces the phenomena.

Image analysis The scripts used for image analysis are available online [2]. The images of the dead-end are flattened to remove the non-uniform lightning by fitting a second-order two-dimensional polynomial to the outside of the channel. Detecting the background is only possible if the fluorescence of the proteins is not much higher than the background fluorescence, otherwise the fluorescence intensity is used as is. The channel sides are detected by using a Scharr edge detection algorithm. Finally the intensity is normalised by the median value of the last five frames in the main channel.

The profiles are extracted by taking the average over the width of the channel, removing one fourth on each side to avoid wall effects. The resulting profile is then filtered using a repeated Savitzki-Golay filter to reduce noise while conserving the shape. Finally, the profiles are plotted

[1] https://doi.org/10.17863/CAM.48786

[2] https://doi.org/10.5281/zenodo.3636078

with a different color for each frame time, as shown in Figure (1).

Finite Elements Simulations A finite elements software was used to simulate the system (Comsol multiphysics 5.2a with Microfluidics module and Optimization module). In one dimension, a Dirichlet boundary condition is used to fix the protein and salt concentration at the inlet of the channel, and a Neumann boundary condition is used on the closed end. In two and three dimensions, the main channel is simulated allowing the main channel flow to enter the dead-end and a local depletion to occur.

Fitting Only profiles with a concentration peak are fitted. As seen on Figure (3), the experimental data fit the profiles well, except in two cases. First, if the peak reaches the end of the channel, the assumption of a semi-infinite channel is clearly broken. Therefore, frames with a significant fluorescence in the last fifth of the channel are not considered. Second, the large intensity difference between the data and the theoretical solution causes the normalised profile to start on a higher level at the channel inlet, as seen on Figure (3). Therefore, the part of the profile between the inlet and the peak is ignored as well. The selected data is illustrated by a solid line, and the ignored data by a dashed line. The solid line is almost completely hidden by the fit.

Free flow electrophoresis and diffusional sizing Free flow electrophoresis is a technique that consists in applying an electric field perpendicularly to the direction of flow and detecting the amount of deviation caused on a stream of particles. The deviation is proportional to the mobility of the particle. Diffusional sizing consists in looking at the diffusion speed under flow and extracting the diffusion coefficient from it. These technique were used to compare the results with

diffusiophoresis. [31,32]

1. Anderson, J. L. & Prieve, D. C. Diffusiophoresis: migration of colloidal particles in gradients of solute concentration. *Separation and Purification Methods* **13**, 67–103 (1984).

2. Anderson, J. L. Colloid transport by interfacial forces. *Annual review of fluid mechanics* **21**, 61–99 (1989).

3. Anderson, J. L. & Prieve, D. C. Diffusiophoresis caused by gradients of strongly adsorbing solutes. *Langmuir* **7**, 403–406 (1991).

4. Derjaguin, B., Dukhin, S. & Korotkova, A. Diffusiophoresis in electrolyte solutions and its role in the mechanism of the formation of films from caoutchouc latexes by the ionic deposition method. *Progress in Surface Science* **43**, 153–158 (1993).

5. Hatch, A., Garcia, E. & Yager, P. Diffusion-based analysis of molecular interactions in microfluidic devices. *Proceedings of the IEEE* **92**, 126–139 (2004).

6. Charmet, J., Arosio, P. & Knowles, T. P. Microfluidics for protein biophysics. *Journal of molecular biology* (2017).

7. Arosio, P. *et al.* Microfluidic diffusion analysis of the sizes and interactions of proteins under native solution conditions. *ACS nano* **10**, 333–341 (2015).

8. Kopp, M. R. & Arosio, P. Microfluidic approaches for the characterization of therapeutic proteins. *Journal of pharmaceutical sciences* (2018).

9. Arosio, P., Hu, K., Aprile, F. A., Müller, T. & Knowles, T. P. Microfluidic diffusion viscometer for rapid analysis of complex solutions. *Analytical chemistry* **88**, 3488–3493 (2016).

10. Abgrall, P. & Gue, A. Lab-on-chip technologies: making a microfluidic network and coupling it into a complete microsystem—a review. *Journal of Micromechanics and Microengineering* **17**, R15 (2007).

11. Sackmann, E. K., Fulton, A. L. & Beebe, D. J. The present and future role of microfluidics in biomedical research. *Nature* **507**, 181–189 (2014).

12. Park, H., Pak, J. J., Son, S. Y., Lim, G. & Song, I. Fabrication of a microchannel integrated with inner sensors and the analysis of its laminar flow characteristics. *Sensors and Actuators A: Physical* **103**, 317–329 (2003).

13. Wu, D., Qin, J. & Lin, B. Electrophoretic separations on microfluidic chips. *Journal of Chromatography A* **1184**, 542–559 (2008).

14. Ugaz, V. M. & Christensen, J. L. Electrophoresis in microfluidic systems. In *Microfluidic Technologies for Miniaturized Analysis Systems*, 393–438 (Springer, 2007).

15. Vigolo, D., Buzzaccaro, S. & Piazza, R. Thermophoresis and thermoelectricity in surfactant solutions. *Langmuir* **26**, 7792–7801 (2010).

16. Vigolo, D., Rusconi, R., Stone, H. A. & Piazza, R. Thermophoresis: microfluidics characterization and separation. *Soft Matter* **6**, 3489–3493 (2010).

17. Ault, J. T., Shin, S. & Stone, H. A. Diffusiophoresis in narrow channel flows. *Journal of Fluid Mechanics* **854**, 420–448 (2018).

18. Shin, S., Ault, J. T., Warren, P. B. & Stone, H. A. Accumulation of colloidal particles in flow junctions induced by fluid flow and diffusiophoresis. *Physical Review X* **7**, 041038 (2017).

19. Hong, J., Kim, B. & Shin, H. Mixed-scale poly (methyl methacrylate) channel network-based single-particle manipulation via diffusiophoresis. *Nanoscale* **10**, 14421–14431 (2018).

20. Shin, S. *et al.* Size-dependent control of colloid transport via solute gradients in dead-end channels. *Proceedings of the National Academy of Sciences* **113**, 257–261 (2016).

21. Shin, S., Ault, J. T., Feng, J., Warren, P. B. & Stone, H. A. Low-cost zeta potentiometry using solute gradients. *Advanced Materials* (2017).

22. Challa, P. K. *et al.* Real-time intrinsic fluorescence visualization and sizing of proteins and protein complexes in microfluidic devices. *Analytical Chemistry* **90**, 3849–3855 (2018). PMID: 29451779.

23. Buffle, J., Zhang, Z. & Startchev, K. Metal flux and dynamic speciation at (bio) interfaces. part i: critical evaluation and compilation of physicochemical parameters for complexes with simple ligands and fulvic/humic substances. *Environmental science & technology* **41**, 7609–7620 (2007).

24. Ault, J. T., Warren, P. B., Shin, S. & Stone, H. A. Diffusiophoresis in one-dimensional solute gradients. *Soft matter* **13**, 9015–9023 (2017).

25. Herling, T. *et al.* Integration and characterization of solid wall electrodes in microfluidic devices fabricated in a single photolithography step. *Applied physics letters* **102**, 184102 (2013).

26. Saar, K. L. *et al.* Rapid two-dimensional characterisation of proteins in solution. *Microsystems & nanoengineering* **5**, 1–10 (2019).

27. Salgin, S., Salgin, U. & Bahadir, S. Zeta potentials and isoelectric points of biomolecules: the effects of ion types and ionic strengths. *Int J Electrochem Sci* **7**, 12404–12414 (2012).

28. Prieve, D. C. & Roman, R. Diffusiophoresis of a rigid sphere through a viscous electrolyte solution. *Journal of the Chemical Society, Faraday Transactions 2: Molecular and Chemical Physics* **83**, 1287–1306 (1987).

29. Prieve, D., Anderson, J., Ebel, J. & Lowell, M. Motion of a particle generated by chemical gradients. part 2. electrolytes. *Journal of Fluid Mechanics* **148**, 247–269 (1984).

30. Challa, P. K., Kartanas, T., Charmet, J. & Knowles, T. P. Microfluidic devices fabricated using fast wafer-scale led-lithography patterning. *Biomicrofluidics* **11**, 014113 (2017).

31. Roman, M. C. & Brown, P. R. Free-flow electrophoresis as a preparative separation technique. *Analytical Chemistry* **66**, 86A–94A (1994).

32. Herling, T. W., Arosio, P., Müller, T., Linse, S. & Knowles, T. P. A microfluidic platform for quantitative measurements of effective protein charges and single ion binding in solution. *Physical Chemistry Chemical Physics* **17**, 12161–12167 (2015).

Acknowledgements The research leading to these results has received funding from the ERC under the European Union Seventh Framework Programme (FP7/2007-2013) through the ERC grant PhysProt (agreement no 337969 T.P.J.K.), and (Q.P.) the European Union's Horizon 2020 research and innovation programme under ETN grant 674979-NANOTRANS. We acknowledge insightful discussions with Professor Daan Frenkel.

Competing Interests The authors declare that they have no competing financial interests.

Correspondence Correspondence and requests for materials should be addressed to T. P. J. K. (email: tpjk2@cam.ac.uk).

Figures

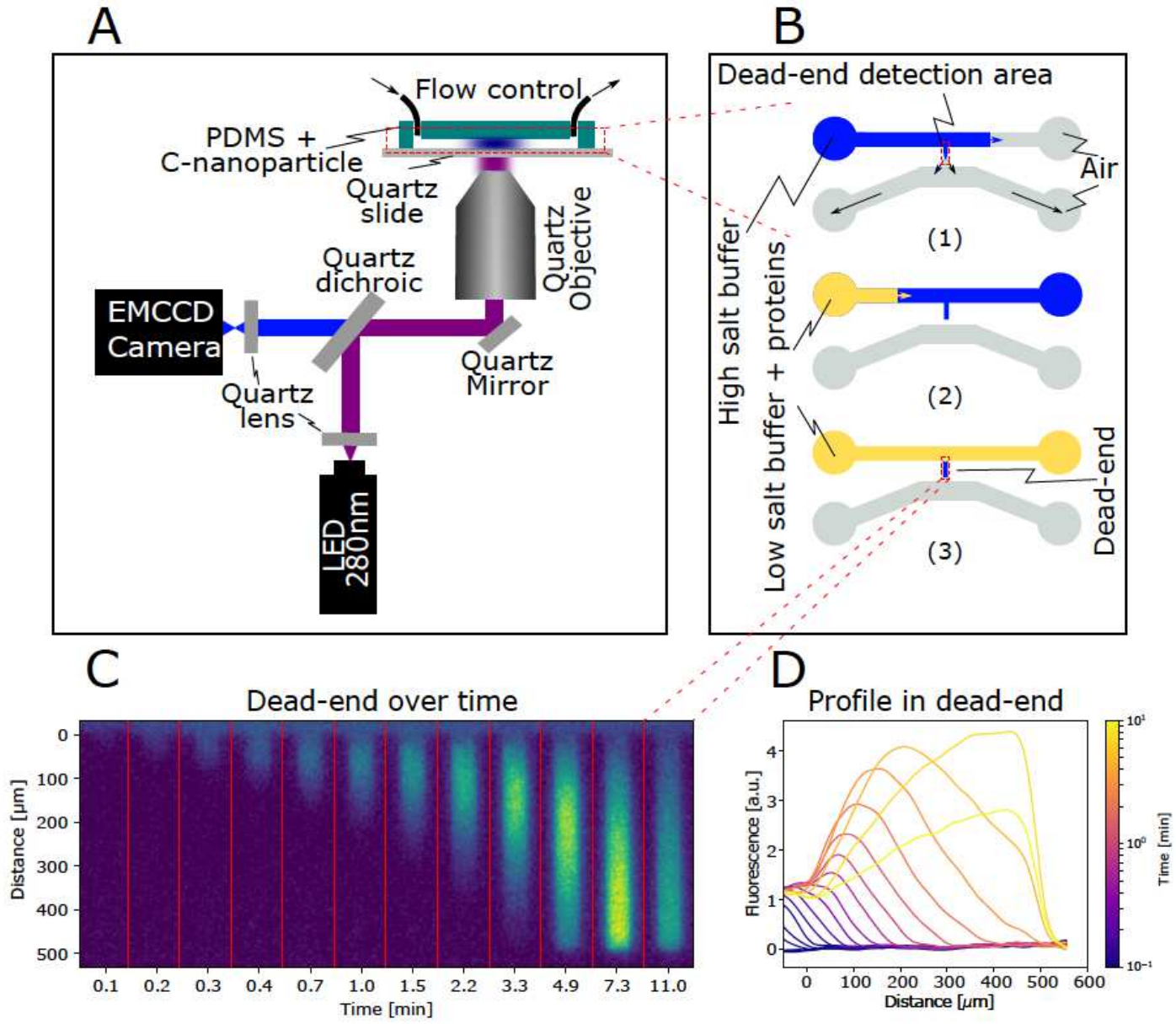

Figure 1

(A) Schematic of the UV label-free microscope used to image a microfluidic device with a dead-end geometry. (B) Microfluidic device design used in this study. (B1) Firstly, the device is filled with a high-salt buffer. The air in the dead-end is pushed through the PDMS in an empty lower channel. (B2) A protein solution is then pushed in the main channel, (B3) leaving the high salt solution only inside the dead-end. (C) A video of the dead-end is taken with logarithmically spaced time points to reduce photobleaching. (D) The channel is detected in each frame and the average over the width is extracted to form a profile.

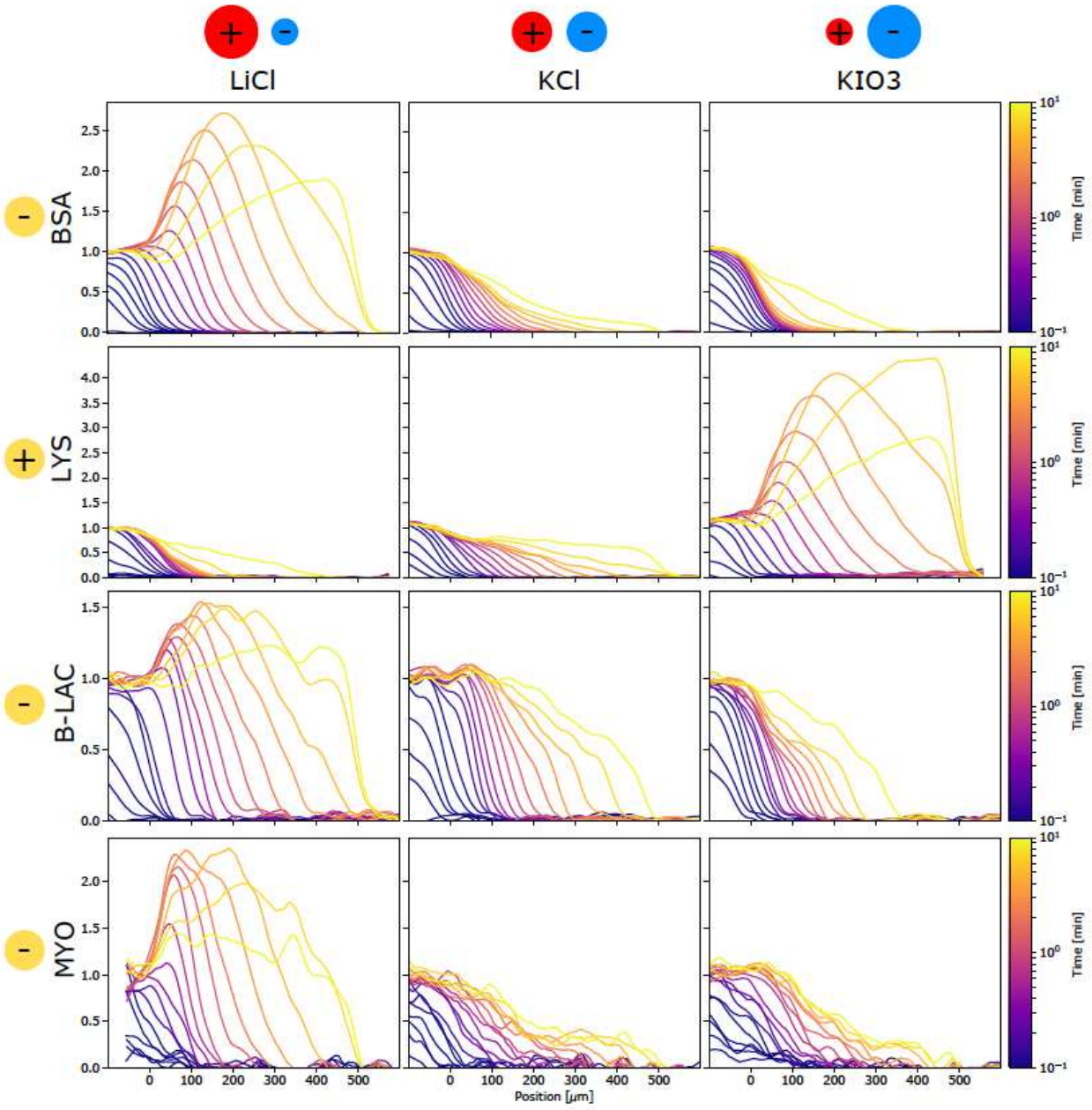

Figure 2

Diffusiophoresis of proteins in different salt gradients. Three negatively charged protein, Bovine Serum Albumin (BSA), Beta-Lactoglobulin (B - LAC), and Myoglobin (MYO), as well as a positively charged protein, Lysozyme (LYS), are placed into a salt gradient. The salts used to create this gradient are Lithium chloride (LiCl), Potassium chloride (KCl), and Potassium iodate (KIO3). If the more diffusive salt ion has the same charge as the protein, a concentration peak appears in the channel. When the more diffusive salt ion has the same charge as the protein, the diffusion in the channel is reduced. If the two ions have similar diffusivity, no effect is visible. A sketch of the ions is shown on top of the figure to help visualize the relative diffusivities, where smaller means more diffusive.

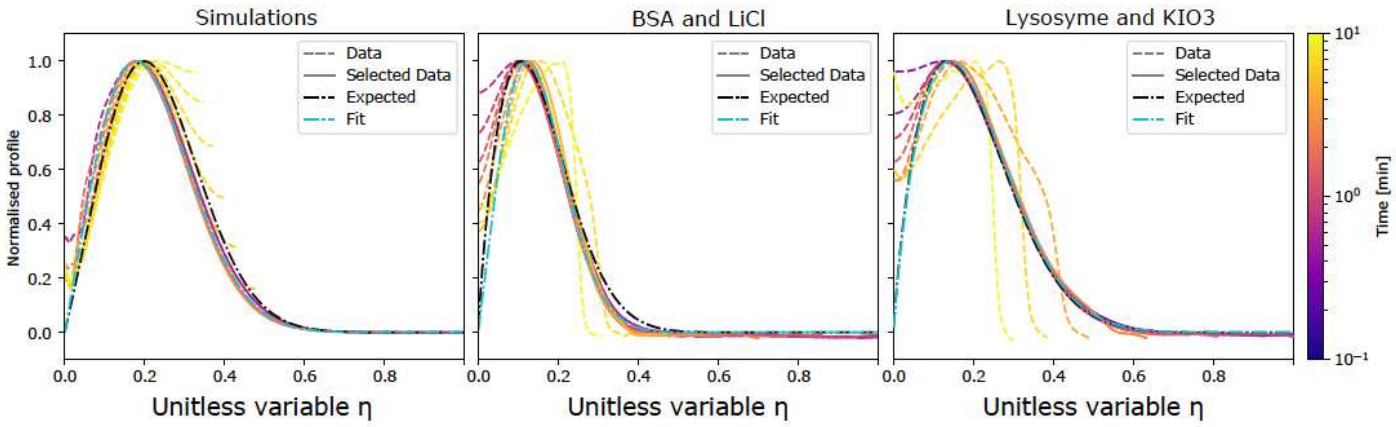

Figure 3

Quantitative description of diffusiophoresis. A finite elements simulation and the two proteins from Figure (2) are plotted as a function of the dimensionless variable . The finite elements simulation and the measurements give similar results. Most curves overlap with the 1D model. The differences are explained by two effects. The main channel is not a perfect reservoir, which can be seen on the left near η = 0. The dead-end channel is not semi-infinite, which is seen by the later, yellow curves not overlapping when reaching the end of the channel. The fitted profile (cyan) and the expected profile (black) both are a good match to the profiles.

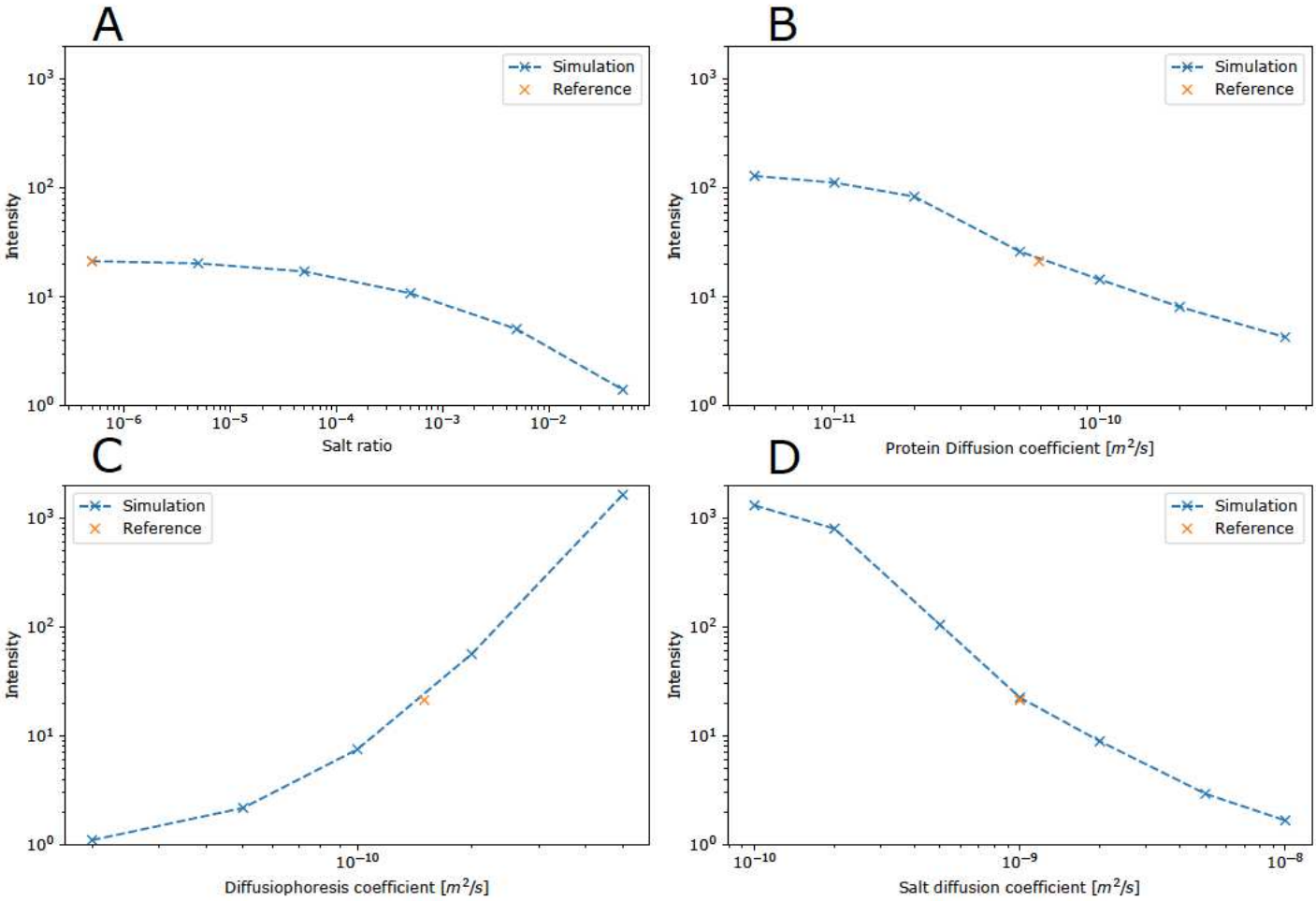

Figure 4

Role of the physical properties of proteins on the strength of the diffusiophoresis effect. The maximum concentration of the simulations is shown as a function of (A) salt ratio, (B) protein diffusion coefficient, (C) diffusiophoresis coefficient, and (D) salt diffusion coefficient. The intensity is the ratio of the maximal concentration with the initial protein concentration. The reference value is the same between the four graphs.

Supplementary Files

This is a list of supplementary files associated with this preprint. Click to download.

- diffusiophoresisSI.pdf